HAL open science

Measurement report: Evolution and distribution of NH3 over Mexico City from ground-based and satellite infrared spectroscopic measurements

Beatriz Herrera, Alejandro Bezanilla, Thomas Blumenstock, Enrico Dammers, Frank Hase, Lieven Clarisse, Adolfo Magaldi, Claudia Rivera, Wolfgang Stremme, Kimberly Strong, et al.

To cite this version:

Beatriz Herrera, Alejandro Bezanilla, Thomas Blumenstock, Enrico Dammers, Frank Hase, et al.. Measurement report: Evolution and distribution of NH3 over Mexico City from ground-based and satellite infrared spectroscopic measurements. Atmospheric Chemistry and Physics, 2022, 22 (21), pp.14119-14132. 10.5194/acp-22-14119-2022 . insu-03661656v2

HAL Id: insu-03661656

https://insu.hal.science/insu-03661656v2

Submitted on 4 Nov 2022

HAL is a multi-disciplinary open access archive for the deposit and dissemination of scientific research documents, whether they are published or not. The documents may come from teaching and research institutions in France or abroad, or from public or private research centers.

L'archive ouverte pluridisciplinaire **HAL**, est destinée au dépôt et à la diffusion de documents scientifiques de niveau recherche, publiés ou non, émanant des établissements d'enseignement et de recherche français ou étrangers, des laboratoires publics ou privés.

Distributed under a Creative Commons Attribution 4.0 International License

Atmos. Chem. Phys., 22, 14119–14132, 2022
https://doi.org/10.5194/acp-22-14119-2022
© Author(s) 2022. This work is distributed under
the Creative Commons Attribution 4.0 License.

Atmospheric Chemistry and Physics
Open Access
EGU

Measurement report: Evolution and distribution of NH_3 over Mexico City from ground-based and satellite infrared spectroscopic measurements

Beatriz Herrera[1,2,3], Alejandro Bezanilla[1], Thomas Blumenstock[4], Enrico Dammers[5], Frank Hase[4], Lieven Clarisse[6], Adolfo Magaldi[7], Claudia Rivera[1], Wolfgang Stremme[1], Kimberly Strong[3], Camille Viatte[8], Martin Van Damme[6,9], and Michel Grutter[1]

[1]Instituto de Ciencias de la Atmósfera y Cambio Climático, Universidad Nacional Autónoma de México, Mexico City 04510, Mexico
[2]Department of Physical and Environmental Sciences, University of Toronto Scarborough, Toronto M1C 1A4, Canada
[3]Department of Physics, University of Toronto, Toronto M5S 1A7, Canada
[4]Karlsruhe Institute of Technology (KIT), Institute of Meteorology and Climate Research (IMK-ASF), Karlsruhe, Germany
[5]Climate, Air and Sustainability (CAS), Netherlands Organisation for Applied Scientific Research (TNO), Utrecht, the Netherlands
[6]Spectroscopy, Quantum Chemistry and Atmospheric Remote Sensing (SQUARES), Université libre de Bruxelles (ULB); Brussels 1050, Belgium
[7]ENES Juriquilla, Universidad Nacional Autónoma de México, Querétaro 762630, Mexico
[8]LATMOS/IPSL, Sorbonne Université, UVSQ, CNRS, Paris, France
[9]Royal Belgian Institute for Space Aeronomy (BIRA-IASB), Brussels, Belgium

Correspondence: Beatriz Herrera (beatriz.herrera@mail.utoronto.ca)

Received: 20 March 2022 – Discussion started: 6 May 2022
Revised: 23 September 2022 – Accepted: 5 October 2022 – Published: 3 November 2022

Abstract. Ammonia (NH_3) is the most abundant alkaline compound in the atmosphere, with consequences for the environment, human health, and radiative forcing. In urban environments, it is known to play a key role in the formation of secondary aerosols through its reactions with nitric and sulfuric acids. However, there are only a few studies about NH_3 in Mexico City. In this work, atmospheric NH_3 was measured over Mexico City between 2012 and 2020 by means of ground-based solar absorption spectroscopy using Fourier transform infrared (FTIR) spectrometers at two sites (urban and remote). Total columns of NH_3 were retrieved from the FTIR spectra and compared with data obtained from the Infrared Atmospheric Sounding Interferometer (IASI) satellite instrument. The diurnal variability of NH_3 differs between the two FTIR stations and is strongly influenced by the urban sources. Most of the NH_3 measured at the urban station is from local sources, while the NH_3 observed at the remote site is most likely transported from the city and surrounding areas. The evolution of the boundary layer and the temperature play a significant role in the recorded seasonal and diurnal patterns of NH_3. Although the vertical columns of NH_3 are much larger at the urban station, the observed annual cycles are similar for both stations, with the largest values in the warm months, such as April and May. The IASI measurements underestimate the FTIR NH_3 total columns by an average of 32.2 ± 27.5 % but exhibit similar temporal variability. The NH_3 spatial distribution from IASI shows the largest columns in the northeast part of the city. In general, NH_3 total columns over Mexico City measured at the FTIR stations exhibited an average annual increase of $92 \pm 3.9 \times 10^{13}$ molecules cm^{-2} yr^{-1} (urban, from 2012 to 2019) and $8.4 \pm 1.4 \times 10^{13}$ molecules cm^{-2} yr^{-1} (remote, from 2012 to 2020), while IASI data within 20 km of the urban station exhibited an average annual increase of $38 \pm 7.6 \times 10^{13}$ molecules cm^{-2} yr^{-1} from 2008 to 2018.

1 Introduction

Atmospheric ammonia (NH_3) is the most abundant basic gas in ambient air (Behera et al., 2013). It predominantly reacts with sulfuric acid (H_2SO_4) and nitric acid (HNO_3) vapour to neutralize a significant fraction of the atmospheric acidity and form ammonium sulfate and ammonium nitrate salts (Seinfeld and Pandis, 2006). Rich NH_3 environments thus promote the formation of secondary inorganic aerosols, which can account for up to 50 % of the mass in the total particular matter (PM) (Behera et al., 2013). $PM_{2.5}$ (PM with an aerodynamic diameter $< 2.5\,\mu m$) is associated with premature human mortality (Paulot and Jacob, 2014; Giannakis et al., 2019), highlighting the importance of taking action to reduce the health impacts due to air pollution, particularly in densely populated environments.

NH_3 has a short lifetime, on the order of hours to a few days (Dammers et al., 2016, 2019; Nair and Yu, 2020; Evangeliou et al., 2021), and exhibits a strong temporal and spatial variability that ranges over three orders of magnitude near the surface (Shephard et al., 2011). NH_3 emissions and deposition strongly depend on environmental conditions. The primary sources of atmospheric NH_3 are related to agricultural activities (mainly livestock and fertilizers), as well as natural sources, biomass burning, vehicular emissions, humans, and pets (Bouwman et al., 1997; Sutton et al., 2008, 2013). Human NH_3 emissions strongly depend on temperature and skin exposure, for example, one adult can emit 0.4 mg of NH_3 per hour at 25 °C but 1.4 of NH_3 per hour at 29 °C (Li et al., 2020). In countries with intensive livestock production, NH_3 is the main contributor to nitrogen fluxes. Emitted NH_3 can be transported by winds and removed from the atmosphere by wet and dry deposition (Neirynck and Ceulemans, 2008; Behera et al., 2013). NH_3 deposition also has an important role in the acidification and eutrophication of ecosystems (Krupa, 2003; Sutton et al., 2008), with multiple effects on water, air, soil, climate, and biodiversity (Sutton et al., 2013).

NH_3 accounts for almost half of all reactive nitrogen released in the atmosphere, with total NH_3 emissions doubling from 1860 to 1993 and possibly doubling again by 2050 (Krupa, 2003; Galloway et al., 2004; Clarisse et al., 2009) mainly driven by the increasing use of fertilizers. Recent advances in satellite remote sensing have resulted in a better knowledge of global NH_3 concentrations, however, uncertainties in the total NH_3 budget, along with the specific emission sources across different spatial scales, remain high mainly due to the lack of observations on land (Clarisse et al., 2009; Behera et al., 2013; Sutton et al., 2013).

The number and size of the world's cities is increasing, with some of them becoming megacities, hosting more than 10 million inhabitants. The urban population worldwide is expected to continue this increase in the coming years, adding about 10 more megacities by 2030 (United Nations, 2018). These massive concentrations of people and their activities present significant challenges for the global environment, especially in terms of air pollution, climate, and human health. One of the largest metropolitan areas in the world, and the largest in North America, is the Mexico City metropolitan area (MCMA), a megacity of > 21 million inhabitants that presents poor air quality during many days of the year. It is located in a basin surrounded by mountains and volcanoes, complicating the ventilation of the polluted air (Molina et al., 2020) that is dominated by the dynamics of the boundary layer (Stremme et al., 2013; Dammers et al., 2016). The Mexico City Emissions Inventory (SEDEMA, 2021) reports that the MCMA hosts almost 6 million vehicles and 1900 regulated industries, and emits a total of 46 931 t of $NH_3\ yr^{-1}$ in the MCMA, including part of the Estado de Mexico. According to the inventory, 0.3 % of NH_3 emissions in Mexico City come from "point sources" such as industry, 5.5 % from "mobile sources" such as vehicles, and 94.2 % from "area sources" including urban waste (1.09 %), agriculture (9.44 %), livestock (13.92 %), and other (69.75 %); within the other category are domestic emissions (69.73 %) and forest fires (0.01 %). The inventory strongly attributes domestic emissions of NH_3 to feces from domesticated animals; in Mexico, the estimated number of dogs and cats is around 23 million with 70 % of them being homeless (GACETA, 2022). Despite the frequent pollution episodes due to PM, the local government has not implemented policies regulating NH_3 emissions.

A few studies have investigated atmospheric NH_3 in the Mexico City area. Surface NH_3 concentrations between 10 and 40 ppbv were measured using an open-path Fourier transform infrared (FTIR) spectrometer, with the highest mixing ratios observed in the morning hours during a 2-month period (Moya et al., 2004). FTIR-NH_3 time series between 2012 and 2015 contributed to a validation study of Infrared Atmospheric Sounding Interferometer (IASI) (Dammers et al., 2016) and Cross-track Infrared Sounder (CrIS) (Dammers et al., 2017) NH_3 satellite products. In terms of NH_3 emissions in Mexico City, Yokelson et al. (2007) reported NH_3 emission factors from forest fires in the mountains surrounding Mexico City in 2006, and Christian et al. (2010) reported emission factors from garbage burning and domestic and industrial biofuel use in central Mexico. A more recent study by Cady-Pereira et al. (2017) investigated the impact of biomass burning events on pollution over the MCMA using trace gas data, including NH_3, from the Tropospheric Emission Spectrometer (TES) instrument onboard the Aura satellite. That study concluded that biomass burning events can impact pollution levels in Mexico City, specifically the south part of the MCMA and particularly during the March–April–May period. Recently, Clarisse et al. (2019) and

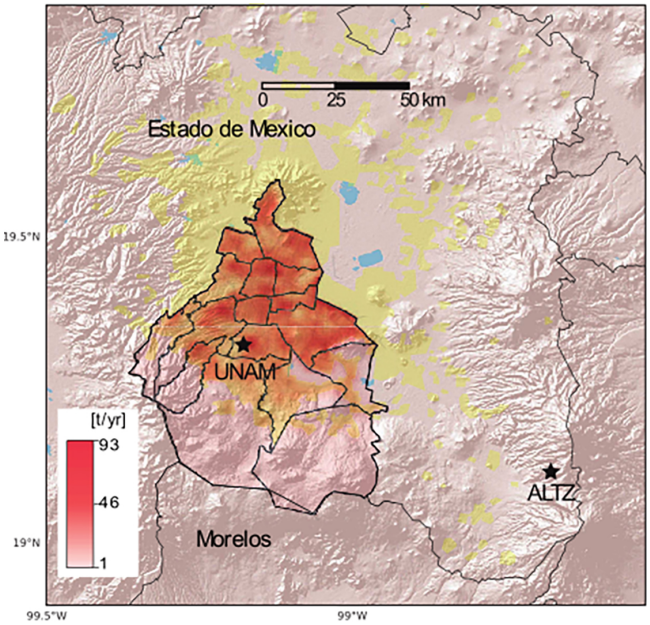

Figure 1. Study area in central Mexico. Mexico City is shown in the middle, with the red shading corresponding to NH_3 emissions reported in the Mexico City Emissions Inventory 2016 (SEDEMA, 2018) in tonnes per year. The stars indicate the location of the Universidad Nacional Autónoma de Mexico (UNAM) and Altzomoni (ALTZ) stations and the yellow shading indicates the extension of the Mexico City metropolitan area (MCMA).

Viatte et al. (2022) reported NH_3 hotspots near Mexico City at Tochtepec (18.84° N, 97.80° W), Ezequiel Montes (20.68° N, 99.93° W), and Tehuacan (18.45° N, 97.31° W), all of which are classified as agricultural sources. Finally, Van Damme et al. (2021) reported an increasing trend of NH_3 over Mexico of $(2.5 \pm 1.5) \times 10^{13}$ molecules cm^{-2} yr^{-1} using 11 years of IASI satellite data (2008–2018).

In this work, the diurnal and seasonal variability of NH_3 over Mexico City is investigated using datasets from two ground-based FTIR spectrometers, including an extension of the FTIR-NH_3 total column time series of the station in Mexico City used in Dammers et al. (2016), and of the FTIR-NH_3 total columns measured at Altzomoni, a remote high-altitude station close to Mexico City, that are retrieved for the first time. The locations of these two sites are shown in Fig. 1. The analysis is complemented with IASI satellite observations over the region, and back-trajectories that were constructed for anomalous NH_3 columns detected at the urban site to assess the influence of local and remote sources.

2 Methodology

2.1 Ground-based FTIR stations and retrieval of NH_3 total columns

This study utilizes NH_3 total columns retrieved from solar absorption spectra measured with ground-based FTIR spectrometers at two sites in and around the MCMA. The urban FTIR station is located at the south of Mexico City within the campus of the Universidad Nacional Autónoma de Mexico on the rooftop of the Instituto de Ciencias de la Atmósfera y Cambio Climático (UNAM, 19.33° N, 99.18° W, 2280 m a.s.l.). A custom-built solar tracker directs solar radiation to the entrance of a FTIR spectrometer (Bruker Optik GmbH model Vertex 80) that has a maximum unapodized resolution of 0.06 cm^{-1}. The instrument is equipped with a KBr beamsplitter and two detectors (HgCdTe and InGaAs). The HgCdTe detector is cooled with liquid nitrogen. For more details about this system, see Bezanilla et al. (2014). Measurements from the remote FTIR site were made at the Altzomoni Atmospheric Observatory (ALTZ, 19.12° N, 98.66° W, 3985 m.a.s.l.), a high-altitude station located 60 km from the UNAM urban site and within the Izta-Popo National Park surrounded by nature. This site is part of the Network for the Detection of Atmospheric Composition Change (NDACC) (De Mazière et al., 2018) contributing data from a high-resolution FTIR spectrometer since 2012. This instrument (Bruker Optik GmbH model IFS 120/125 HR) can record solar spectra with a maximum spectral resolution of 0.0035 cm^{-1}, and is equipped with KBr and CaF_2 beamsplitters and HgCdTe, InSb, and InGaAs detectors. For details of the site and the instrument, see Baylon et al. (2017). The first study presenting and validating the combined usage of trace gas products obtained from dedicated retrievals with FTIR spectra measured at UNAM and ALTZ was that of Plaza-Medina et al. (2017).

The FTIR spectra used for the retrieval of NH_3 were collected with the HgCdTe detector at both sites with a spectral resolution of 0.005 cm^{-1} at Altzomoni, and 0.1 cm^{-1} (prior to 2014) and 0.075 cm^{-1} at UNAM, using an optical band pass filter to enhance the region between 700 and 1400 cm^{-1}. In this study, we extend the UNAM time series used in a previous 2012–2015 comparison between IASI and FTIR (Dammers et al., 2016) with improvements to the retrieval, and we present for the first time Altzomoni FTIR-NH_3 retrievals for the period between April 2012 and May 2020. The analysis presented here focuses on the region around the MCMA, also using the IASI satellite product and a back-trajectory evaluation, as described below.

For both sites, the solar FTIR spectra were analysed using PROFFIT version 9.6 for the retrievals (Hase et al., 2004) to obtain the NH_3 total columns. A retrieval strategy based on that reported by Dammers et al. (2015) was used, comprising two microwindows (929.1–931.8 and 963.7–970.0 cm^{-1}) to cover the NH_3 absorption lines from the υ_2 vibrational

band in the mid-IR region. The trace gases H_2O, CO_2, O_3, CO, and N_2O were taken into account as interfering species for the retrieval for both stations, and the temperature and pressure profiles were obtained from the US National Centers for Environmental Prediction (NCEP). Spectroscopic parameters were obtained from the high-resolution transmission molecular absorption database HITRAN 2008 Rothman et al., 2009), and the a priori profile information about the interfering gases was obtained from 40-year averages of simulations from the Whole Atmosphere Community Climate Model (WACCM) (Eyring et al., 2007; Marsh et al., 2013). Since NH_3 profiles from WACCM are only representative of remote regions, scaled a priori profiles derived from 5 years of averaged NH_3 simulations from the global chemical transport model GEOS-Chem v11 were used instead. Constructed scaled a priori profiles have been used previously from GEOS-Chem simulations for the retrieval of trace gases (Shephard et al., 2011; Shephard and Cady-Pereira, 2015; Bader et al., 2017). A total of 7992 NH_3 columns were retrieved for the UNAM station and 4031 for ALTZ. The resulting uncertainties obtained with PROFFIT averaged over the entire time series in molecules cm^{-2} at UNAM were 1.25×10^{15} (random), 8.40×10^{14} (systematic), and 1.52×10^{15} or 11.50 % (total); and 3.09×10^{14} (random), 3.14×10^{14} (systematic), and 4.42×10^{14} or 51.37 % (total) at ALTZ. The average degrees of freedom for signal (DOFS) averaged over the entire time series were 2.03 for UNAM and 1.04 for ALTZ.

2.2 IASI-NH_3 data product and comparison methodology

IASI measures the infrared thermal radiation emitted by the Earth's surface and the atmosphere from a Sun-synchronous orbit on board the MetOp platform. Spectra are recorded in the 645–2760 cm^{-1} spectral range at a spectral resolution of 0.5 cm^{-1} (Clerbaux et al., 2009). The instrument crosses the Equator at mean local solar times of 09:30 LT and 21:30 LT providing global coverage of the Earth twice a day. IASI has a field-of-view composed of four circular footprints each with a diameter of 12 km at the nadir view and up to 20 km × 39 km elliptical pixels outside the nadir depending on the satellite viewing angle, complemented by scanning along a swath width of 2200 km off-nadir perpendicular to the ground track (Clarisse et al., 2009; Van Damme et al., 2014, 2015). The IASI-NH_3 retrieval products are based on artificial neural networks (ANNs) that link the hyperspectral range index (HRI), a calculated dimensionless index that represents the amount of NH_3 in the column, to other input parameters such as temperature, pressure, water vapour profiles, and parameterized vertical profiles of NH_3 to derive the NH_3 total column. The algorithm maps the HRI to the NH_3 total column using a trained neural network; the uncertainty of each NH_3 column can be estimated by the propagation of the input parameters' uncertainties. However, large HRI values (more than 3σ) are associated to a confident detection of NH_3 (Van Damme et al., 2014, 2017 Whitburn et al., 2016). The current spectral range for the retrieval process is set to 812–1126 cm^{-1} to increase the sensitivity of NH_3 and reduce interferences (Van Damme et al., 2021). The retrieval scheme does not produce averaging kernels, however previous studies comparing the IASI-NH_3 product with ground-based FTIR measurements have demonstrated good agreement (e.g. Dammers et al., 2016, 2017; Lutsch et al., 2019; Tournadre et al., 2020; Yamanouchi et al., 2021). In addition, under conditions of high NH_3 and when the thermal contrast is large, IASI has maximum sensitivity to NH_3 in the boundary layer (Clarisse et al., 2010). An error estimate is provided with each individual IASI observation; for this work IASI observations with errors less than 100 % were used. IASI's average detection limit for NH_3 under large thermal contrast is about 3 ppbv, and can be as low as 1 ppbv under conditions of well-mixed NH_3 throughout a thick boundary layer (Clarisse et al., 2010).

For this study, 11 years of the IASI-A NH_3 total columns (ANNs for IASI (ANNI)-NH_3-v3) between 2008–2018 were used; details of this version 3 can be found in Appendix A of Van Damme et al. (2021), and was also used by Yamanouchi et al. (2021) and Viatte et al. (2022). The spatial distribution of NH_3 over Mexico City was obtained by averaging all the IASI-A morning observations between January 2008 and December 2018 over this region. The FTIR-NH_3 total columns at UNAM were compared against the IASI-NH_3 total columns over Mexico City to assess the agreement between both data sets. Due to the high spatiotemporal variability of NH_3, the temporal and spatial coincidence criteria were tested and assessed using the correlations (both R and slope). In addition, as suggested in Dammers et al. (2016), an elevation filter (FTIR station altitude minus IASI observation < 300 m) was applied. The criteria resulting in the best correlations were elevation filter < 300 m, spatial sampling difference < 20 km, maximum temporal sampling difference ± 40 min, and maximum IASI-NH_3 retrieval error of 100 %. The seasonal variability comparison and annual averages were performed using only FTIR-NH_3 retrievals between 09:00 LT and 10:59 LT, corresponding to the IASI overpass time over Mexico City, and the < 20 km spatial criterion for IASI-NH_3 total columns. Altzomoni correlation plots with IASI-NH_3 data were not included due to the few coincidences between the FTIR and IASI.

2.3 Back-trajectory analysis

To determine the primary sources of NH_3 measured at the UNAM station and to assess the dominant atmospheric transport pathways during the events with the largest hourly means of the NH_3 columns in the time series, trajectory cluster analysis (Reizer and Orza, 2018) was applied. Back-trajectories of 8 h were selected to capture the air masses passing over the MCMA. Using the UNAM station as the

receptor, back-trajectories were calculated using the Hybrid Single-Particle Lagrangian Integrated Trajectory (HYSPLIT) model (Stein et al., 2015; Draxler et al., 1997) at different altitudes above the UNAM station level (2280 m a.s.l.). The HYSPLIT model can be run online at the following link https://www.ready.noaa.gov/HYSPLIT.php (last access: 21 October 2022). The wind data used for the back-trajectories were derived from the NCEP North American Mesoscale (NAM) analysis product at 12 km and 1 h of spatial and temporal resolution, respectively (NCEPT NAM, 2015). The cluster analysis is an embedded routine in HYSPLIT and is based on the Ward's agglomerative hierarchical clustering algorithm (Ward, 1963). Finally, the total spatial variance (TSV) method (Draxler et al., 2021), included in HYSPLIT, was used to fit the number of clusters that represent the data.

3 Results and discussion

3.1 FTIR-NH_3 time series and temporal variability

The NH_3 total column time series retrieved at both FTIR stations are shown in Fig. 2. The urban UNAM columns, shown in the top panel, are about one order of magnitude larger than the high-altitude Altzomoni columns. The average NH_3 total columns for the entire period ($1.46 \pm 0.64 \times 10^{16}$ at UNAM and $1.87 \pm 2.40 \times 10^{15}$ molecules cm^{-2} at Altzomoni) are listed and compared to values reported for stations in other parts of the world in Table 1. The Mexico City NH_3 total columns are comparable with those reported in Bremen, while they are about twice as large as those measured at Toronto (Canada), Paris (France), and Lauder (New Zealand). Jungfraujoch, a remote high-altitude station in Switzerland with similar characteristics to Altzomoni, presents a significantly lower average NH_3 column and also has much lower variability. The reason for this might be that Altzomoni is impacted more frequently by biomass burning events in the dry season and also by the regional boundary layer, receiving polluted air from Mexico City and other large urban centres in the afternoon (Baumgardner et al., 2009).

Figure 2 also shows the fit of a Fourier series (Baylon et al., 2017) to reproduce seasonality in both stations. A clear cycle is seen at both stations, with a maximum between mid- and late April, and a minimum in late December. However, the difference between the minimum and the maximum is larger at Altzomoni, with UNAM having greater NH_3 background concentrations. The average annual increase in the NH_3 columns obtained from the Fourier fit are $92 \pm 3.9 \times 10^{13}$ at UNAM (from 2012 to 2019) and $8.4 \pm 1.4 \times 10^{13}$ molecules cm^{-2} yr^{-1} at Altzomoni (from 2012 to 2020). Van Damme et al. (2021) reported a trend from 2008 to 2018 of $2.5 \pm 1.5 \times 10^{13}$ molecules cm^{-2} yr^{-1} for all of Mexico, which is closer to the Altzomoni value. The difference in magnitude can be attributed to the datasets and methodology as the present study uses ground-based FTIR measurements from two sites with higher values in 2019 and 2020, while Van Damme et al. (2021) used IASI satellite data over a wider region between 2008 to 2018.

The average diurnal variability of the FTIR NH_3 total columns at both stations is displayed in Fig. 3. The largest average NH_3 columns at the urban station are on the order of 1.50×10^{16} molecules cm^{-2} and were observed during the morning and the evening. Although the diurnal pattern is not as evident as in other cities where motor vehicles have been found to be a dominant source of urban NH_3 (e.g., Osada et al., 2019; Kotnala et al., 2020), traffic emissions in Mexico City still might play a role in conjunction with other urban sources of atmospheric NH_3. The average NH_3 columns at UNAM have a minimum of 1.35×10^{16} molecules cm^{-2} at 13 h, which can be attributed to the conversion to ammonium, as was observed by Moya et al. (2004) when describing the evolution of the surface gas phase NH_3 and PM NH_4^+ at an urban site in Mexico City.

The diurnal cycle at the remote station (Fig. 3a) is noticeably different, with NH_3 columns that increase systematically as the day progresses, with the largest variability in the afternoon hours. Altzomoni is located within a natural protected area with few local sources of NH_3, and even less so during the morning hours when values are around 0.10×10^{16} molecules cm^{-2}, when cooler temperatures do not favour the volatilization of NH_3. The columns increase throughout the day, having the largest average values of 0.76×10^{16} molecules cm^{-2} in the evening, probably transported from lower altitudes by the dynamics of the regional boundary layer (Baumgardner et al., 2009). This is supported by the large variability observed in the afternoon, since the probability that NH_3 is transported > 1700 m a.g.l. (above ground level) up to this site strongly depends on the meteorological conditions, which vary from day to day. Comparisons between daily average NH_3 columns and the daily averages of some meteorological variables from the RUOA Network (Red Universitaria de Observatorios Atmosféricos), such as temperature, relative humidity (RH), precipitation, and solar radiation, resulted in weak correlations. These correlations were positive with temperature and solar radiation (r between 0.1 and 0.3), and negative with RH and precipitation (r between -0.1 and -0.3). The average wind speed for Altzomoni is 4.5 m s^{-1}, with dominant winds from the east-southeast and west-northwest, while the average wind speed for UNAM is 1.6 m s^{-1}, with dominant winds from the north and the north-northwest.

The seasonal variability of the FTIR NH_3 total columns is shown in Fig. 4. In general, the pattern is similar at both stations, showing the NH_3 temperature dependence with larger NH_3 columns in the months of March, April, and May which correspond to the warm–dry season; this season usually has days with clear skies, weak winds, high pressure systems, and biomass burning events (Molina et al., 2020), and also corresponds to the most critical part of the fire season in Mexico City (CENAPRED, 2021; Yokelson et al., 2007). In addition, there are two agricultural seasons in the country,

Table 1. Mean NH_3 total columns reported from ground-based FTIR stations.

Station	Location	Time period	Average NH_3 total column (molecules cm^{-2}) $\times 10^{15}$	Station characteristics	Reference
Bremen, Germany	53.10° N, 8.85° E 27 m a.s.l.	2004–2013	13.7 ± 4.24	Urban, fertilizers, livestock	Dammers et al. (2015)
Paris, France	48.79° N, 2.44° E, 56 m a.s.l.	2009–2017	8.4 ± 8.6	Urban, surrounding agricultural sources	Tournadre et al. (2020)
Jungfraujoch, Switzerland	46.55° N, 7.98° E, 3580 m a.s.l.	2004–2013	0.18 ± 0.07	Remote and high altitude, no large sources	Dammers et al. (2015)
Toronto, Canada	43.66° N, 79.40° W, 174 m a.s.l.	2002–2005 2015–2018	5.94 ± 5.14 8.13 ± 7.88	Urban, fertilizers, biomass burning	Yamanouchi et al. (2021)
UNAM, Mexico	19.33° N, 99.18° W, 2280 m a.s.l.	2012–2019	14.6 ± 6.39	Urban, large sources	This study
Altzomoni, Mexico	19.12° N, 98.66° W, 3985 m a.s.l.	2012–2020	1.87 ± 2.40	Remote and high altitude, no local sources, biomass burning	This study
Reunion, Indian Ocean	20.90° S, 55.5° E, 85 m a.s.l.	2004–2012	0.80 ± 0.54	Remote, fertilizers, fires	Dammers et al. (2015)
Lauder, New Zealand	45.04° S, 169.68° E, 370 m a.s.l.	2004–2014	4.17 ± 1.40	Remote, fertilizer, livestock	Dammers et al. (2015)

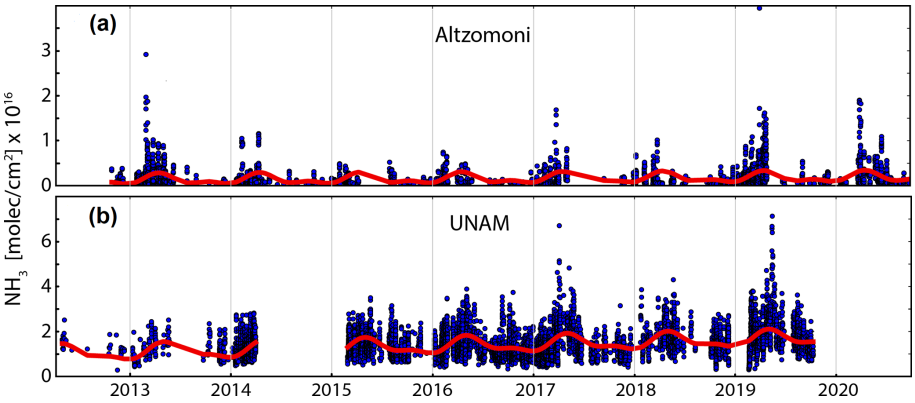

Figure 2. Time series of retrieved FTIR-NH_3 data over **(a)** Altzomoni and **(b)** UNAM, with a fitted Fourier series (red) to reproduce seasonality. Note the differences in magnitude.

the first one from April to September and the second one from October to March. The fertilizer application combined with meteorological conditions could favour NH_3 volatilization from the agricultural sources contributing to the higher NH_3 spring columns observed in Fig. 4. Smaller columns are clearly observed during the wet season (June to October), due to the increase in wet deposition, and during the cold–dry season from November to February, due to less favourable conditions for NH_3 volatilization. This is in agreement with Viatte et al. (2022). The annual cycle of NH_3 columns at the urban UNAM station is similar to that observed at the background Altzomoni station but has a larger amplitude. A study by Sun et al. (2017) observed that the growing efficiency of three-way catalysts in motor vehicles is responsible for large NH_3 emissions detected in urban locations in the USA and China. These emissions are strongly dependent on traffic volume and thus should not have a strong seasonality. On the other hand, emissions originating from agricultural activity usually have a distinct seasonality that depends on the fertilizer application and temperature (Sun et al., 2017; Van Damme et al., 2015, Viatte et al., 2022). In the current study, the annual cycles follow the pattern of temperature (Fig. 4c), indicating that emissions from other sources, such as fires, waste treatment, human or pets emissions, may be contributing significantly to the NH_3 detected over the MCMA.

There are more features to note in Fig. 4. While Altzomoni and UNAM NH_3 columns have similar annual cycles, those at Altzomoni have greater variability throughout the differ-

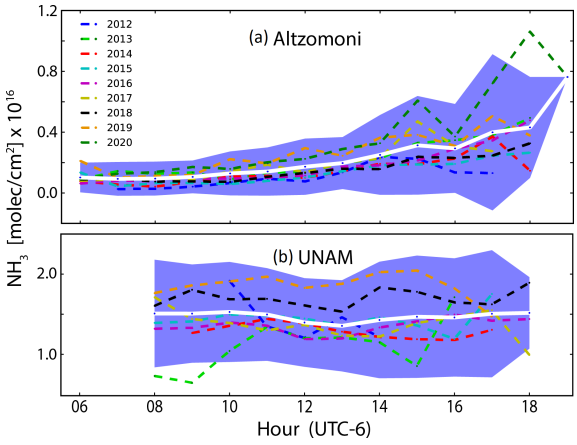

Figure 3. Average diurnal evolution of NH_3 total columns over Mexico City at **(a)** Altzomoni and **(b)** UNAM. Different years are shown in different colours, the thick white line is the average for all years, and the blue shading indicates $\pm 1\sigma$.

ent years during the warm–dry season than during the rest of the year. This might be due to the strong relationship between pollutants reaching the high-altitude station and the boundary layer dynamics and wind conditions, which are more variable during the warm–dry season. However, another contribution to this variability may be biomass burning activity, which has a maximum during the warm–dry months as has been shown by Cady-Pereira et al. (2017). The 2013 pollution events presented by Cady-Pereira et al. (2017) are seen on 23 April, 9 May, and 25 May in Fig. 2, with 9 May having the largest enhancements at Altzomoni; unfortunately, there are no coincident measurements for UNAM. At Altzomoni, the average NH_3 column for 9 May 2013 was $2.39 \pm 0.53 \times 10^{15}$ molecules cm^{-2}, which is 28 % greater than the average column for the entire period (Table 1). However, in 2013, the largest NH_3 column measured at Altzomoni was on the evening of 27 February with an average value of $17.4 \pm 0.58 \times 10^{15}$ molecules cm^{-2}, almost 10 times higher than the average column presented in Table 1. This enhancement on 27 February 2013 seems to be local and of short duration, most likely due to a nearby biomass burning event. This is supported by the detection of active fires northwest of the site on that date by the MODIS instrument on Aqua as shown in Fig. 5. With its high altitude and few local sources, Altzomoni seems to be more sensitive for the detection of pollution events than UNAM. Even if the fires are not occurring nearby, the increased lifetimes of emitted pollutants at these altitudes may favour transport over longer distances to Altzomoni.

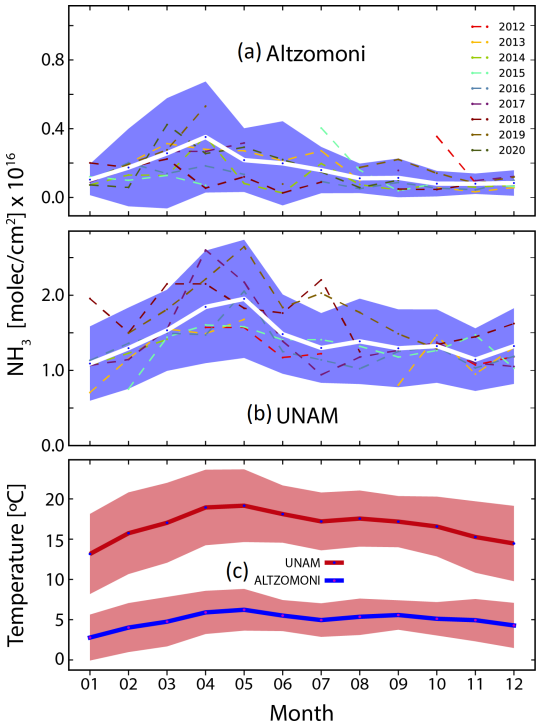

Figure 4. Monthly averages showing annual cycle of NH_3 over Mexico City at **(a)** Altzomoni and **(b)** UNAM. The thick white line is the average for all years and the shading indicates $\pm 1\sigma$. **(c)** Monthly averages of temperature at both stations between 2014–2018 for Altzomoni and 2012–2018 for UNAM. The shaded area indicates $\pm 1\sigma$.

3.2 Satellite observations: comparison with ground-based measurements and spatial distribution

The correlation between IASI-NH_3 and the ground-based FTIR-NH_3 total columns at UNAM from November 2013 to December 2018 is shown in Fig. 6. The coincidence criteria are described in Sect. 2.2, and are based on values used in previous validations of IASI products using ground-based FTIR data (Dammers et al., 2016), including an elevation correction using the Space Shuttle Radar Topography Mission Global Product at 3 arcsec resolution over Mexico City (SRTMGL3, Farr et al., 2007). A total of 64 coincident data pairs were found, from which a correlation coefficient $R = 0.72$ and a mean relative difference (MRD) of -32.2 ± 27.5 % were obtained ($\pm 1\sigma$). These results are consistent with $R = 0.64$ and MRD $= -30.8 \pm 43.9$ % reported by Dammers et al. (2016) for this region using an older version of the IASI-NH_3 product. The correlation is also similar to that of Tournadre et al. (2020), who obtained $R = 0.79$, when comparing IASI-NH_3 to FTIR-NH_3 columns using a similar instrument (Vertex 80) in Paris, and to the $R = 0.80$ and MRD $= -32.4 \pm 56.3$ % reported for 547 coincidences from several ground-based FTIR stations

Figure 5. Snapshot of Mexico City's fire events on 27 February 2013, from the Aqua MODIS instrument with true colour-corrected reflectance and resolution of 25 m, obtained from NASA Worldview Snapshots (https://earthdata.nasa.gov, last access: 21 October 2022). The red dots show the fire events. The stars indicate the location of the UNAM and Altzomoni stations.

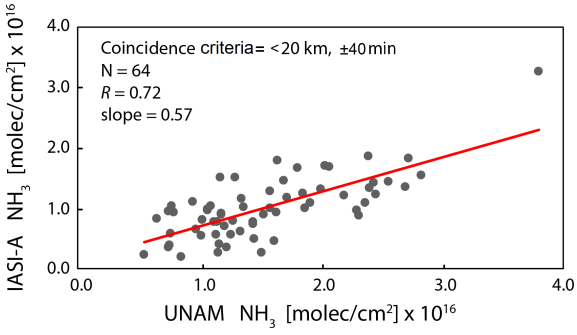

Figure 6. Correlation plot for IASI-A NH_3 vs. UNAM FTIR-NH_3 total columns, with coincidence criteria of < 20 km, ± 40 min, elevation (FTIR station – IASI observation) < 300 m, IASI-NH_3 retrieval error < 100 % between November 2013 and December 2018.

and IASI-NH_3 (Dammers et al., 2016). The ANNI-NH_3-v3 product is thus in agreement with the ground-based data and even presents an improved correlation compared to the previous result. However, an underestimation in the IASI-NH_3 total columns of approximately 32 % over Mexico City persists. Dammers et al. (2017), using an older version of the ANNI-NH_3 product, attributed these differences to a combination of more randomly distributed error sources and large systematic errors, however these reasons need to be investigated further.

The spatial distribution of NH_3 over MCMA as observed by IASI is presented in Fig. 7. The distribution shows a clear NH_3 enhancement in the northeast section of Mexico City and in part of the Estado de México region. There are several potentially important sources located in this area: Mexico City International Airport, an area of continuous traffic emissions; the Bordo Poniente compost plant, which treats around 1500 t of daily organic waste from the city; wastewater discharge and treatment bodies with nearby bird colonies such as the regulation lagoon Cola de Pato; and the agricultural area at Texcoco. The combination of these factors, along with the high population density of this area, are likely to be cause of the NH_3 enhancements observed in this part of the city. This enhancement is partially in agreement with the location of the larger NH_3 emissions reported in the Mexico City Emissions Inventory (SEDEMA, 2018, 2021) shown in Fig. 1 in the northern part of the city, which is mainly associated with population activities and domestic animals' excreta. Figure 7d will be discussed in Sect. 3.3.

Figure 7a–c shows the variations of NH_3 over the year, with the largest columns measured during the warm–dry season and to the northeast of UNAM. In contrast, the NH_3 columns are reduced in the wet season when wet deposition can occur, and are smallest during the cold–dry season, when there are lower temperatures and less NH_3 volatilization. To investigate the influence of local topography on the NH_3 distribution, Fig. 8 compares the average IASI-NH_3 total column spatial distribution (a) with altitude (b). The figure illustrates that the highest columns are located at the lowest altitudes while the lowest columns are at higher altitudes, reflecting the source locations and the boundary layer dynamics. The figure shows that the main NH_3 sources in MCMA are located in the most urbanized areas in Mexico City and Estado de Mexico at an altitude of around 2250 m. These urban emissions agree with the statement of Li et al. (2020) that human NH_3 emissions contribute significantly to the total NH_3 emissions in hot and highly populated urban areas such as Mexico City. A rough estimation using 25 °C as an average diurnal temperature for Mexico City and the 0.4 mg of NH_3 per hour at 25 °C from Li et al. (2020) resulted in an estimate of 34 t of NH_3 per year, a contribution of the same order of magnitude as all the "point sources" and "urban waste" combined according to the Mexico City Emissions Inventory (SEDEMA, 2018, 2021).

Comparisons between the seasonal and temporal variability of NH_3 over the UNAM station in Mexico City were performed using morning (9–11 h) FTIR-NH_3 columns and IASI-NH_3 columns with a spatial criterion of < 20 km from the UNAM station (Fig. 9a). The NH_3 seasonal variability over Mexico City in Fig. 9a is similar for both the IASI and ground-based FTIR NH_3 columns and is in agreement with Fig. 4. However, IASI-NH_3 shows a consistent negative bias. The evolution with time is represented by the IASI-NH_3 and FTIR-NH_3 annual averages in Fig. 9b. The datasets suggest an increasing trend in the annual averages of the NH_3 to-

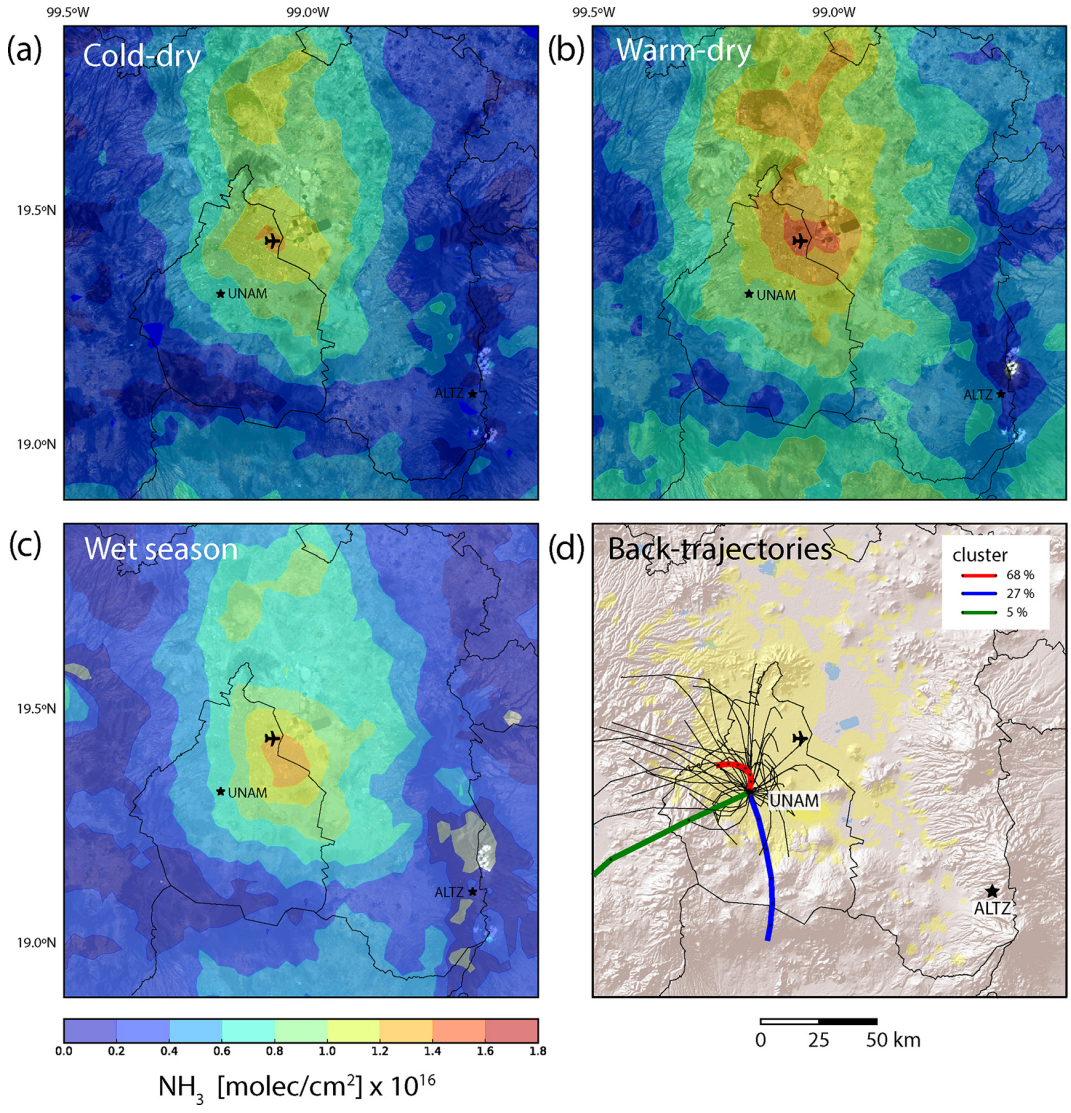

Figure 7. Spatial distribution of IASI-A NH_3 total columns for the morning overpass of MetOp-A over Mexico City, averaged over 2008–2018 for **(a)** the cold–dry season (November–February), **(b)** the warm–dry season (March–May), and **(c)** the wet season (June–October). HYSPLIT back-trajectories for the UNAM site are shown in panel **(d)**. The black stars indicate the locations of both stations, and Mexico City International Airport is shown for reference.

tal columns, with larger columns observed in the most recent years, even in Altzomoni, except for 2013 which was affected by the 27 February event as discussed previously. The average annual increase of the IASI-NH_3 columns between 2008 and 2018 (using the < 20 km spatial criterion and the same Fourier fit as for the FTIR data) is $38 \pm 7.6 \times 10^{13}$ molecules cm^{-2} yr^{-1} for Mexico City. This is a larger positive trend than that of $2.5 \pm 1.5 \times 10^{13}$ molecules cm^2 yr^{-1} reported by Van Damme et al. (2021) for all of Mexico over the same period, but lies between the values obtained for the remote and urban FTIR measurements.

3.3 Back-trajectory analysis and origin of observed NH_3 in Mexico City

A cluster analysis was applied using 8 h back-trajectories 100 m above UNAM station to identify the main transport pathways for air masses arriving at this station that correspond to the highest average hourly NH_3 total columns (Fig. 7d). The 100 m cluster was considered the most representative because NH_3 is mostly concentrated near the surface. The TSV method was able to represent the primary trajectories at 100 m above UNAM with only three clusters. It was found that 68 % of the trajectories originate from the north (red line with black dots), 27 % from the west-southwest (green line), and 5 % from the south (blue line).

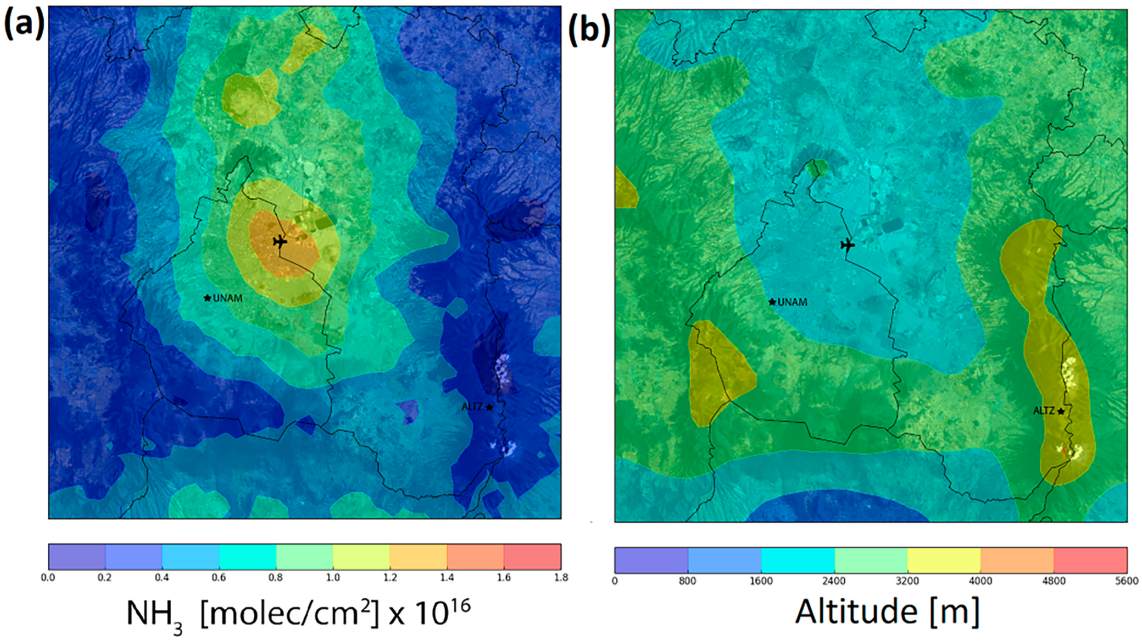

Figure 8. Spatial distribution of **(a)** IASI-A NH_3 total columns for the morning overpass of MetOp-A over Mexico City, averaged over 2008–2018 **(b)** altitudes in Mexico City from the Space Shuttle Radar Topography Mission Global product City (SRTMGL3, Farr et al., 2007). The black stars indicate the location of ground-based stations, and Mexico City International Airport is shown for reference.

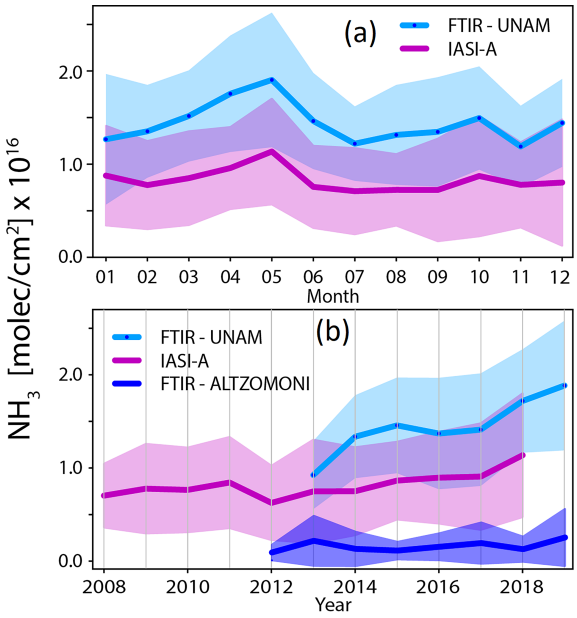

Figure 9. IASI and FTIR NH_3 total columns with coincidence criteria of < 20 km and < 2 h: **(a)** monthly averages at UNAM, **(b)** annual averages at UNAM and Altzomoni. The shaded area indicates $\pm 1\sigma$.

However, the individual back-trajectories that comprise the red cluster (the thin black lines in Fig. 7d) indicate that most of the NH_3 detected at UNAM comes from a variety of local sources and does not originate exclusively from NH_3-enriched air masses transported from the enhancement region to the northeast observed in Fig. 7a–c. This is in agreement with Viatte et al. (2022). The relationship between the back-trajectories and measured NH_3 columns can be explained by the fact that Mexico City is located in a basin; the wind fields are constricted in this basin and in general they are breeze winds ($6\,km\,h^{-1}$). Under these conditions, small locally distributed NH_3 urban emissions seem to be the main cause of the high column values of this pollutant measured at the UNAM station, this agrees with Fig. 8 which shows that the main NH_3 sources in MCMA seem to be urban.

4 Conclusions

This work presented the temporal and spatial distribution of NH_3 total columns over the Mexico City metropolitan area derived from two ground-based FTIR spectrometers and IASI satellite observations. The average NH_3 total column at the urban UNAM site ($1.46 \pm 0.64 \times 10^{16}$ molecules cm^{-2}) is considerably higher than that at the remote station Altzomoni ($1.87 \pm 2.40 \times 10^{15}$ molecules cm^{-2}), with a clear difference in the diurnal cycle but similar seasonal variability. NH_3 spatial distribution from IASI shows the highest NH_3 columns in the northeast part of the city, an area surrounded by water bodies, a landfill, a compost plant for the

treatment of the organic waste, and the airport. The IASI ANNI-NH_3-v3 data product underestimates the NH_3 total columns over Mexico City, with a mean relative difference of 32 %, over the period 2008–2018 but showed a similar temporal variability and a good correlation with FTIR measurements ($R = 0.72$). The analysis of back-trajectories for the largest NH_3 enhancement events suggests that most of the NH_3 measured at the urban station is coming from local sources. The NH_3 observed at the remote site is most likely transported from the surroundings and it is influenced by biomass burning events. These results present evidence that sources other than from agriculture, such as motor vehicles, fires, human emissions, domestic animals, water discharge, and waste, have a significant contribution to the total NH_3 budget in the city. In general, an average annual increase is observed in Mexico City from both ground-based stations ($92 \pm 3.9 \times 10^{13}$ molecules cm^{-2} yr^{-1} at UNAM, $8.4 \pm 1.4 \times 10^{13}$ molecules cm^{-2} yr^{-1} at Altzomoni) and IASI ($38 \pm 7.6 \times 10^{13}$ molecules cm^{-2} yr^{-1}). A complementary study using surface NH_3 and PM concentrations from passive samplers and microsensors around this region is in progress. These observations, together with model data, will examine the role of reactive nitrogen in the pollution of Mexico City. A revaluation of NH_3 emission sources contribution in the Mexico City inventory is suggested. Measures to mitigate NH_3 emissions and reduce these positive trends are important, given that NH_3 is closely linked to secondary aerosol formation and the deterioration of ecosystems.

Data availability. The UNAM and Altzomoni FTIR data used in this study are available at https://doi.org/10.5281/zenodo.7199948 (Herrera et al., 2022). The meteorological data for both FTIR stations are available at https://www.ruoa.unam.mx/csv_data/unam/minuto.php (RUOA, 2022a) and https://www.ruoa.unam.mx/csv_data/altz/minuto.php (RUOA, 2022b). The IASI ANNI-NH_3-v3 L2 data are freely available and can be accessed through the AERIS database at https://iasi.aeris-data.fr/NH3/ (AERIS, 2022). MODIS active fire snapshots are available at https://wvs.earthdata.nasa.gov/ (NASA, 2022). The code of the HYSPLIT model can be obtained from https://www.arl.noaa.gov/hysplit/getrun-hysplit/ (NOAA, 2022). Last access to all URLs: 14 October 2022.

Author contributions. BH is the main author of the paper, analysed the data, made most of the figures, and wrote the text. WS contributed to the data analysis. MG contributed to create some figures. AM contributed with the back-trajectory analysis. MG, KS, CR, FH, TB, CV, ED, LC, and MVD contributed to the paper writing and provided support. AB provided technical support. ED provided the Space Shuttle Radar Topography Mission Global product and support with the NH_3 retrievals. LC and MVD developed the IASI-NH_3 product. CV and MVD provided the IASI data. All authors reviewed the paper.

Competing interests. The contact author has declared that none of the authors has any competing interests.

Disclaimer. Publisher's note: Copernicus Publications remains neutral with regard to jurisdictional claims in published maps and institutional affiliations.

Acknowledgements. We acknowledge the use of imagery from the Worldview Snapshots application (https://wvs.earthdata.nasa.gov, last access: 14 October 2022), part of the Earth Observing System Data and Information System (EOSDIS). Beatriz Herrera acknowledges CONACYT for the scholarship granted. The RUOA Network (https://www.ruoa.unam.mx, last access: 14 October 2022) is acknowledged for making the meteorological measurements available. IASI is a joint mission of EUMETSAT and the Centre National d'Etudes Spatiales (CNES, France). The authors acknowledge the ULB-LATMOS team for providing the IASI data and for the development of the retrieval algorithms. We thank Miguel Ángel Robles Roldan for building the solar tracker at UNAM and his technical assistance.

Financial support. This research has been supported by the Consejo Nacional de Ciencia y Tecnología (CONACYT) (PhD grant no. 665043).

Review statement. This paper was edited by Jayanarayanan Kuttippurath and reviewed by two anonymous referees.

References

AERIS: NH_3 total column from IASI (Level 2), https://iasi.aeris-data.fr/NH3/, last access: 14 October 2022.

Bader, W., Bovy, B., Conway, S., Strong, K., Smale, D., Turner, A. J., Blumenstock, T., Boone, C., Collaud Coen, M., Coulon, A., Garcia, O., Griffith, D. W. T., Hase, F., Hausmann, P., Jones, N., Krummel, P., Murata, I., Morino, I., Nakajima, H., O'Doherty, S., Paton-Walsh, C., Robinson, J., Sandrin, R., Schneider, M., Servais, C., Sussmann, R., and Mahieu, E.: The recent increase of atmospheric methane from 10 years of ground-based NDACC FTIR observations since 2005, Atmos. Chem. Phys., 17, 2255–2277, https://doi.org/10.5194/acp-17-2255-2017, 2017.

Baumgardner, D., Grutter, M., Allan, J., Ochoa, C., Rappenglueck, B., Russell, L. M., and Arnott, P.: Physical and chemical properties of the regional mixed layer of Mexico's Megapolis, Atmos. Chem. Phys., 9, 5711–5727, https://doi.org/10.5194/acp-9-5711-2009, 2009.

Baylon, J. L., Stremme, W., Grutter, M., Hase, F., and Blumenstock, T.: Background CO2 levels and error analysis from ground-based solar absorption IR measurements in central Mexico, Atmos. Meas. Tech., 10, 2425–2434, https://doi.org/10.5194/amt-10-2425-2017, 2017.

Behera, S. N., Sharma, M., Aneja, V. P., and Balasubramanian, R.: Ammonia in the atmosphere: A review on emission sources, atmospheric chemistry and deposition on ter-

restrial bodies, Environ. Sci. Pollut. R., 20, 8092–8131, https://doi.org/10.1007/s11356-013-2051-9, 2013.

Bezanilla, A., Krüger, A., Stremme, W., and Grutter, M.: Solar absorption infrared spectroscopic measurements over Mexico City: Methane enhancements, Atmósfera, 27, 173–183, https://doi.org/10.1016/S0187-6236(14)71108-7, 2014.

Bouwman, A F, Lee, D. S., Asman, W. A. H., Dentener, F. J., Van Der Hoek, K. W., and Olivier, J. G. J.: A global high-resolution emission inventory for ammonia, Global Biogeochem. Cy., 11, 561–587, 1997.

Cady-Pereira, K. E., Payne, V. H., Neu, J. L., Bowman, K. W., Miyazaki, K., Marais, E. A., Kulawik, S., Tzompa-Sosa, Z. A., and Hegarty, J. D.: Seasonal and spatial changes in trace gases over megacities from Aura TES observations: two case studies, Atmos. Chem. Phys., 17, 9379–9398, https://doi.org/10.5194/acp-17-9379-2017, 2017.

CENAPRED Centro Nacional de prevención de Desastres: Incendios Forestales, http://www.cenapred.gob.mx/es/Publicaciones/archivos/159-FASCCULOINCENDIOSFORESTALES.PDF (last access: 21 October 2022), 2021.

Christian, T. J., Yokelson, R. J., Cárdenas, B., Molina, L. T., Engling, G., and Hsu, S.-C.: Trace gas and particle emissions from domestic and industrial biofuel use and garbage burning in central Mexico, Atmos. Chem. Phys., 10, 565–584, https://doi.org/10.5194/acp-10-565-2010, 2010.

Clarisse, L., Clerbaux, C., Dentener, F., Hurtmans, D., and Coheur, P. F.: Global ammonia distribution derived from infrared satellite observations, Nat. Geosci., 2, 479–483, https://doi.org/10.1038/ngeo551, 2009.

Clarisse, L., Shephard, M. W., Dentener, F., Hurtmans, D., Cady-Pereira, K., Karagulian, F., Van Damme, M., Clerbaux, C., and Coheur, P. F.: Satellite monitoring of ammonia: A case study of the San Joaquin Valley, J. Geophys. Res.-Atmos., 115, 1–15, https://doi.org/10.1029/2009JD013291, 2010.

Clarisse, L., Van Damme, M., Clerbaux, C., and Coheur, P.-F.: Tracking down global NH3 point sources with wind-adjusted superresolution, Atmos. Meas. Tech., 12, 5457–5473, https://doi.org/10.5194/amt-12-5457-2019, 2019.

Clerbaux, C., Boynard, A., Clarisse, L., George, M., Hadji-Lazaro, J., Herbin, H., Hurtmans, D., Pommier, M., Razavi, A., Turquety, S., Wespes, C., and Coheur, P.-F.: Monitoring of atmospheric composition using the thermal infrared IASI/MetOp sounder, Atmos. Chem. Phys., 9, 6041–6054, https://doi.org/10.5194/acp-9-6041-2009, 2009.

Dammers, E., Vigouroux, C., Palm, M., Mahieu, E., Warneke, T., Smale, D., Langerock, B., Franco, B., Van Damme, M., Schaap, M., Notholt, J., and Erisman, J. W.: Retrieval of ammonia from ground-based FTIR solar spectra, Atmos. Chem. Phys., 15, 12789–12803, https://doi.org/10.5194/acp-15-12789-2015, 2015.

Dammers, E., Palm, M., Van Damme, M., Vigouroux, C., Smale, D., Conway, S., Toon, G. C., Jones, N., Nussbaumer, E., Warneke, T., Petri, C., Clarisse, L., Clerbaux, C., Hermans, C., Lutsch, E., Strong, K., Hannigan, J. W., Nakajima, H., Morino, I., Herrera, B., Stremme, W., Grutter, M., Schaap, M., Wichink Kruit, R. J., Notholt, J., Coheur, P.-F., and Erisman, J. W.: An evaluation of IASI-NH3 with ground-based Fourier transform infrared spectroscopy measurements, Atmos. Chem. Phys., 16, 10351–10368, https://doi.org/10.5194/acp-16-10351-2016, 2016.

Dammers, E., Shephard, M. W., Palm, M., Cady-Pereira, K., Capps, S., Lutsch, E., Strong, K., Hannigan, J. W., Ortega, I., Toon, G. C., Stremme, W., Grutter, M., Jones, N., Smale, D., Siemons, J., Hrpcek, K., Tremblay, D., Schaap, M., Notholt, J., and Erisman, J. W.: Validation of the CrIS fast physical NH_3 retrieval with ground-based FTIR, Atmos. Meas. Tech., 10, 2645–2667, https://doi.org/10.5194/amt-10-2645-2017, 2017.

Dammers, E., McLinden, C. A., Griffin, D., Shephard, M. W., Van Der Graaf, S., Lutsch, E., Schaap, M., Gainairu-Matz, Y., Fioletov, V., Van Damme, M., Whitburn, S., Clarisse, L., Cady-Pereira, K., Clerbaux, C., Coheur, P. F., and Erisman, J. W.: NH_3 emissions from large point sources derived from CrIS and IASI satellite observations, Atmos. Chem. Phys., 19, 12261–12293, https://doi.org/10.5194/acp-19-12261-2019, 2019.

De Mazière, M., Thompson, A. M., Kurylo, M. J., Wild, J. D., Bernhard, G., Blumenstock, T., Braathen, G. O., Hannigan, J. W., Lambert, J.-C., Leblanc, T., McGee, T. J., Nedoluha, G., Petropavlovskikh, I., Seckmeyer, G., Simon, P. C., Steinbrecht, W., and Strahan, S. E.: The Network for the Detection of Atmospheric Composition Change (NDACC): history, status and perspectives, Atmos. Chem. Phys., 18, 4935–4964, https://doi.org/10.5194/acp-18-4935-2018, 2018.

Draxler, R. R. and Hess, G. D.: Description of the HYSPLIT_4 modeling system. NOAA Tech. Memo. ERL ARL-224, NOAA Air Resources Laboratory, Silver Spring, MD, 24 pp., https://www.arl.noaa.gov/wp_arl/wp-content/uploads/documents/reports/arl-224.pdf (last access:21 October 2022), 1997.

Draxler, R. R., Stunder, B., Rolph, G., Stein, A., and Taylor, A.: HYSPLIT User's Guide. Silver Spring, Maryland, USA, NOAA Air Resources Laboratory, http://www.arl.noaa.gov/documents/reports/hysplit_user_guide.pdf (last access: 21 October 2022), 2021.

Evangeliou, N., Balkanski, Y., Eckhardt, S., Cozic, A., Van Damme, M., Coheur, P.-F., Clarisse, L., Shephard, M. W., Cady-Pereira, K. E., and Hauglustaine, D.: 10-year satellite-constrained fluxes of ammonia improve performance of chemistry transport models, Atmos. Chem. Phys., 21, 4431–4451, https://doi.org/10.5194/acp-21-4431-2021, 2021.

Eyring, V., Waugh, D. W., Bodeker, G. E., Cordero, E., Akiyoshi, H., Austin, J., Beagley, S. R., Boville, B. A., Braesicke, P., Brühl, C., Butchart, N., Chipperfield, M. P., Dameris, M., Deckert, R., Deushi, M., Frith, S. M., Garcia, R. R., Gettelman, A., Giorgetta, M. A., Kinnison, D. E., Mancini, E., Manzini, E., Marsh, D. R., Matthes, S., Nagashima, T., Newman, P. A., Nielsen, J. E., Pawson, S., Pitari, G., Plummer, D. A., Rozanov, E., Schraner, M., Scinocca, J. F., Semeniuk, K., Shepherd, T. G., Shibata, K., Steil, B., Stolarski, R. S., Tian, W., and Yoshiki, M.: Multimodel projections of stratospheric ozone in the 21st century, J. Geophys. Res.-Atmos., 112, D16303, https://doi.org/10.1029/2006JD008332, 2007.

Farr, T. G., Rosen, P. A., Caro, E., and Crippen, R.: The Shuttle Radar Topography Mission, Rev. Geophys., 45, RG2004, https://doi.org/10.1029/2005RG000183, 2007.

GACETA: LXIV/1PPO-56/86584, https://www.senado.gob.mx/64/gaceta_del_senado/documento/86584, last access: 2 September 2022.

Galloway, J. N., Dentener, F. J., Capone, D. G., Boyer, E. W., Howarth, R. W., Seitzinger, S. P., Asner, G. P., Cleveland, C.

C., Green, P. A., Holland, E. A., Karl, D. M., Michaels, A. F., Porter, J. H., Townsend, A. R., and Vörösmarty, C. J.: Nitrogen cycles: past, present, and future, Biogeochemistry, 70, 153–226, https://doi.org/10.1007/s10533-004-0370-0, 2004.

Giannakis, E., Kushta, J., Bruggeman, A., and Lelieveld, J.: Costs and benefits of agricultural ammonia emission abatement options for compliance with European air quality regulations, Environ. Sci. Eur., 31, 93, https://doi.org/10.1186/s12302-019-0275-0, 2019.

Hase, F., Hannigan, J. W., Coffey, M. T., Goldman, A., Höpfner, M., Jones, N. B., Rinsland, C. P., and Wood, S. W.: Intercomparison of retrieval codes used for the analysis of high-resolution, ground-based FTIR measurements, J. Quant. Spectrosc. Ra., 87, 25–52, https://doi.org/10.1016/j.jqsrt.2003.12.008, 2004.

Herrera, B., Bezanilla, A., Blumenstock, T., Dammers, E., Hase, F., Clarisse, L., Magaldi, A., Rivera, C., Stremme, W., Strong, K., Viatte, C., Van Damme, M., and Grutter, M.: Replication data for Measurement report: Evolution and distribution of NH_3 over Mexico City from ground-based and satellite infrared spectroscopic measurements, Zenodo [data set], https://doi.org/10.5281/zenodo.7199948, 2022.

Kotnala, G., Sharma, S. K., and Mandal, T. K.: Influence of Vehicular Emissions (NO, NO_2, CO and NMHCs) on the Mixing Ratio of Atmospheric Ammonia (NH_3) in Delhi, India, Arch. Environ. Con. Tox., 78, 79–85, https://doi.org/10.1007/s00244-019-00689-8, 2020.

Krupa, S. V.: Effects of atmospheric ammonia (NH_3) on terrestrial vegetation: A review, Environ. Pollut., 124, 179–221, https://doi.org/10.1016/S0269-7491(02)00434-7, 2003.

Li, M., Weschler, C. J., Bekö, G., Wargocki, P., Lucic, G., and Williams, J.: Human Ammonia Emission Rates under Various Indoor Environmental Conditions, Environ. Sci. Technol., 54, 5419–5428, https://doi.org/10.1021/acs.est.0c00094, 2020.

Lutsch, E., Strong, K., Jones, D. B. A., Ortega, I., Hannigan, J. W., Dammers, E., Shephard, M. W., Morris, E., Murphy, K., Evans, M. J., Parrington, M., Whitburn, S., Van Damme, M., Clarisse, L., Coheur, P. F., Clerbaux, C., Croft, B., Martin, R. V., Pierce, J. R., and Fisher, J. A.: Unprecedented Atmospheric Ammonia Concentrations Detected in the High Arctic From the 2017 Canadian Wildfires, J. Geophys. Res.-Atmos., 124, 8178–8202, https://doi.org/10.1029/2019JD030419, 2019.

Marsh, D. R., Mills, M. J., Kinnison, D. E., Lamarque, J. F., Calvo, N., and Polvani, L. M.: Climate change from 1850 to 2005 simulated in CESM1(WACCM), J. Climate, 26, 7372–7391, https://doi.org/10.1175/JCLI-D-12-00558.1, 2013.

Molina, L. T., Lei, W., Zavala, M., Almanza, V., Garcia, A., Saide, P., and Mena-Carrasco, M.: Atmospheric Pollution: Experience from Mexico City and Santiago de Chile, in: Air Pollution Modeling and its Application XXVI, 127–138, https://doi.org/10.1007/978-3-030-22055-6_21, 2020.

Moya, M., Grutter, M., and Báez, A.: Diurnal variability of size-differentiated inorganic aerosols and their gas-phase precursors during January and February of 2003 near downtown Mexico City, Atmos. Environ., 38, 5651–5661, https://doi.org/10.1016/j.atmosenv.2004.05.045, 2004.

Nair, A. A. and Yu, F.: Quantification of Atmospheric Ammonia Concentrations: A Review of Its Measurement and Modeling, Atmosphere, 11, 1092, https://doi.org/10.3390/atmos11101092, 2020.

NASA: Worldview Snapshots, https://wvs.earthdata.nasa.gov/, last access: 14 October 2022.

NCEP NAM: National Centers for Environmental Prediction/National Weather Service/NOAA/U.S. Department of Commerce. NCEP North American Mesoscale (NAM) 12 km Analysis. Research Data Archive at the National Center for Atmospheric Research, Computational and Information Systems Laboratory [data set], https://doi.org/10.5065/G4RC-1N91, 2015.

Neirynck, J. and Ceulemans, R.: Bidirectional ammonia exchange above a mixed coniferous forest, Environ. Pollut., 154, 424–438, https://doi.org/10.1016/j.envpol.2007.11.030, 2008.

NOAA: Get & Run HYSPLIT, https://www.arl.noaa.gov/hysplit/getrun-hysplit/, last access: 14 October 2022.

Osada, K., Saito, S., Tsurumaru, H., and Hoshi, J.: Vehicular exhaust contributions to high NH_3 and $PM_{2.5}$ concentrations during winter in Tokyo, Japan, Atmos. Environ., 206, 218–224, https://doi.org/10.1016/j.atmosenv.2019.03.008, 2019.

Paulot, F. and Jacob, D. J.: Hidden cost of U.S. agricultural exports: Particulate matter from ammonia emissions, Environ. Sci. Technol., 48, 903–908, https://doi.org/10.1021/es4034793, 2014.

Plaza-Medina, E. F., Stremme, W., Bezanilla, A., Grutter, M., Schneider, M., Hase, F., and Blumenstock, T.: Ground-based remote sensing of O_3 by high- and medium-resolution FTIR spectrometers over the Mexico City basin, Atmos. Meas. Tech., 10, 2703–2725, https://doi.org/10.5194/amt-10-2703-2017, 2017.

Red Universitaria de Observatorios Atmosféricos (RUOA): Datos de cada minuto para el observatorio atmosferico UNAM, https://www.ruoa.unam.mx/csv_data/unam/minuto.php, last access: 14 October 2022a.

Red Universitaria de Observatorios Atmosféricos (RUOA): Datos de cada minuto para el observatorio atmosferico Altzomoni, https://www.ruoa.unam.mx/csv_data/altz/minuto.php, last access: 14 October 2022b.

Reizer, M. and Orza, J. A. G.: Identification of PM_{10} air pollution origins at a rural background site, E3S Web Conf., 28, 1–7, https://doi.org/10.1051/e3sconf/20182801031, 2018.

Rothman, L. S., Gordon, I. E., Barbe, A., Benner, D. C., Bernath, P. F., Birk, M., Boudon, V., Brown, L. R., Campargue, A., Champion, J. P., Chance, K., Coudert, L. H., Dana, V., Devi, V. M., Fally, S., Flaud, J. M., Gamache, R. R., Goldman, A., Jacquemart, D., Kleiner, I., Lacome, N., Lafferty, W. J., Mandin, J. Y., Massie, S. T., Mikhailenko, S. N., Miller, C. E., Moazzen-Ahmadi, N., Naumenko, O. V., Nikitin, A. V., Orphal, J., Perevalov, V. I., Perrin, A., Predoi-Cross, A., Rinsland, C. P., Rotger, M., Šimečková, M., Smith, M. A. H., Sung, K., Tashkun, S. A., Tennyson, J., Toth, R. A., Vandaele, A. C., and Vander Auwera, J.: The HITRAN 2008 molecular spectroscopic database, J. Quant. Spectrosc. Ra., 110, 533–572, https://doi.org/10.1016/j.jqsrt.2009.02.013, 2009.

SEDEMA Secretaría del Medio Ambiente de la Ciudad de México: Inventario de Emisiones de la Ciudad de México 2016, Dirección General de Gestión de la Calidad del Aire, Dirección de Programas de Calidad del Aire e Inventario de Emisiones, Ciudad de México, http://www.aire.cdmx.gob.mx/descargas/publicaciones/flippingbook/inventario-emisiones-2016/mobile/inventario-emisiones-2016.pdf (last access: 21 October 2022), 2018.

SEDEMA Secretaría del Medio Ambiente de la Ciudad de México: Inventario de Emisiones de la Zona Metropolitana del Valle de

México 2018, Dirección General de Gestión de la Calidad del Aire, Dirección de Proyectos de Calidad del Aire, Ciudad de México, http://www.aire.cdmx.gob.mx/descargas/publicaciones/flippingbook/memoria-inventario-emisiones-2018/memoria_inventario_emisiones_2018.pdf (last access: 21 October 2022), 2021.

Seinfeld, J. H. and Pandis, S. N.: Atmospheric Chemistry and Physics: From Air Pollution to Climate Change, 2nd Edn., John Wiley, New York, 2006.

Shephard, M. W. and Cady-Pereira, K. E.: Cross-track Infrared Sounder (CrIS) satellite observations of tropospheric ammonia, Atmos. Meas. Tech., 8, 1323–1336, https://doi.org/10.5194/amt-8-1323-2015, 2015.

Shephard, M. W., Cady-Pereira, K. E., Luo, M., Henze, D. K., Pinder, R. W., Walker, J. T., Rinsland, C. P., Bash, J. O., Zhu, L., Payne, V. H., and Clarisse, L.: TES ammonia retrieval strategy and global observations of the spatial and seasonal variability of ammonia, Atmos. Chem. Phys., 11, 10743–10763, https://doi.org/10.5194/acp-11-10743-2011, 2011.

Stein, A. F., Draxler, R. R., Rolph, G. D., Stunder, B. J. B., Cohen, M. D., and Ngan, F.: NOAA's HYSPLIT atmospheric transport and dispersion modeling system, B. Am. Meteorol. Soc., 96, 2059–2077, https://doi.org/10.1175/BAMS-D-14-00110.1, 2015.

Stremme, W., Grutter, M., Rivera, C., Bezanilla, A., Garcia, A. R., Ortega, I., George, M., Clerbaux, C., Coheur, P. F., Hurtmans, D., Hannigan, J. W., and Coffey, M. T.: Top-down estimation of carbon monoxide emissions from the Mexico Megacity based on FTIR measurements from ground and space, Atmos. Chem. Phys., 13, 1357–1376, https://doi.org/10.5194/acp-13-1357-2013, 2013.

Sun, K., Tao, L., Miller, D. J., Pan, D., Golston, L. M., Zondlo, M. A., Griffin, R. J., Wallace, H. W., Leong, Y. J., Yang, M. M., Zhang, Y., Mauzerall, D. L., and Zhu, T.: Vehicle Emissions as an Important Urban Ammonia Source in the United States and China, Environ. Sci. Technol., 51, 2472–2481, https://doi.org/10.1021/acs.est.6b02805, 2017.

Sutton, M. A., Erisman, J. W., Dentener, F., and Möller, D.: Ammonia in the environment: From ancient times to the present, Environ. Pollut., 156, 583–604, https://doi.org/10.1016/j.envpol.2008.03.013, 2008.

Sutton, M. A., Reis, S., Riddick, S. N., Dragosits, U., Nemitz, E., Theobald, M. R., Tang, Y. S., Braban, C. F., Vieno, M., Dore, A. J., Mitchell, R. F., Wanless, S., Daunt, F., Fowler, D., Blackall, T. D., Milford, C., Flechard, C. R., Loubet, B., Massad, R., Cellier, P., Personne, E., Coheur, P. F., Clarisse, L., Van Damme, M., Ngadi, Y., Clerbaux, C., Skjøth, C. A., Geels, C., Hertel, O., Kruit, R. J. W., Pinder, R. W., Bash, J. O., Walker, J. T., Simpson, D., Horváth, L., Misselbrook, T. H., Bleeker, A., Dentener, F., and de Vries, W.: Towards a climate-dependent paradigm of ammonia emission and deposition, Philos. T. Roy. Soc. B, 368, 20130166, https://doi.org/10.1098/rstb.2013.0166, 2013.

Tournadre, B., Chelin, P., Ray, M., Cuesta, J., Kutzner, R. D., Landsheere, X., Fortems-Cheiney, A., Flaud, J.-M., Hase, F., Blumenstock, T., Orphal, J., Viatte, C., and Camy-Peyret, C.: Atmospheric ammonia (NH_3) over the Paris megacity: 9 years of total column observations from ground-based infrared remote sensing, Atmos. Meas. Tech., 13, 3923–3937, https://doi.org/10.5194/amt-13-3923-2020, 2020.

United Nations: The World 's Cities in 2018, World's Cities 2018 – Data Bookl. (ST/ESA/ SER.A/417), 34, https://www.un.org/en/development/desa/population/publications/pdf/urbanization/the_worlds_cities_in_2018_data_booklet.pdf (last access: 21 October 2022), 2018.

Van Damme, M., Wichink Kruit, R. J., Schaap, M., Clarisse, L., Clerbaux, C., Coheur, P. F., Dammers, E., Dolman, A. J., and Erisman, J. W.: Evaluating 4 years of atmospheric ammonia (NH_3) over Europe using IASI satellite observations and LOTOS-EUROS model results, J. Geophys. Res., 119, 9549–9566, https://doi.org/10.1002/2014JD021911, 2014.

Van Damme, M., Erisman, J. W., Clarisse, L., Dammers, E., Whitburn, S., Clerbaux, C., Dolman, A. J., and Coheur, P.: Worldwide spatiotemporal atmospheric ammonia (NH_3), Geophys. Res. Lett., 42, 1–9, https://doi.org/10.1002/2015GL065496, 2015.

Van Damme, M., Whitburn, S., Clarisse, L., Clerbaux, C., Hurtmans, D., and Coheur, P. F.: Version 2 of the IASI NH_3 neural network retrieval algorithm: Near-real-time and reanalysed datasets, Atmos. Meas. Tech., 10, 4905–4914, https://doi.org/10.5194/amt-10-4905-2017, 2017.

Van Damme, M., Clarisse, L., Franco, B., Sutton, M. A., Erisman, J. W., Wichink Kruit, R., Van Zanten, M., Whitburn, S., Hadji-Lazaro, J., Hurtmans, D., Clerbaux, C., and Coheur, P. F.: Global, regional and national trends of atmospheric ammonia derived from a decadal (2008–2018) satellite record, Environ. Res. Lett., 16, 055017, https://doi.org/10.1088/1748-9326/abd5e0, 2021.

Viatte, C., Abeed, R., Yamanouchi, S., Porter, W., Safieddine, S., Van Damme, M., Clarisse, L., Herrera, B., Grutter, M., Coheur, P.-F., Strong, K., and Clerbaux, C.: NH_3 spatiotemporal variability over Paris, Mexico and Toronto and its link to $PM_{2.5}$ during pollution events, EGUsphere [preprint], https://doi.org/10.5194/egusphere-2022-413, 2022.

Ward, J: Hierarchical Grouping to Optimize an Objective Function, J. Am. Stat. Assoc., 58, 236–244, https://doi.org/10.1080/01621459.1963.10500845, 1963.

Whitburn, S., Van Damme, M., Clarisse, L., Bauduin, S., Heald, C. L., Hadji-Lazaro, J., Hurtmans, D., Zondlo, M. A., Clerbaux, C., and Coheur, P. F.: A flexible and robust neural network IASI-NH_3 retrieval algorithm, J. Geophys. Res., 121, 6581–6599, https://doi.org/10.1002/2016JD024828, 2016.

Yamanouchi, S., Viatte, C., Strong, K., Lutsch, E., Jones, D. B. A., Clerbaux, C., Van Damme, M., Clarisse, L., and Coheur, P.-F.: Multiscale observations of NH_3 around Toronto, Canada, Atmos. Meas. Tech., 14, 905–921, https://doi.org/10.5194/amt-14-905-2021, 2021.

Yokelson, R. J., Urbanski, S. P., Atlas, E. L., Toohey, D. W., Alvarado, E. C., Crounse, J. D., Wennberg, P. O., Fisher, M. E., Wold, C. E., Campos, T. L., Adachi, K., Buseck, P. R., and Hao, W. M.: Emissions from forest fires near Mexico City, Atmos. Chem. Phys., 7, 5569–5584, https://doi.org/10.5194/acp-7-5569-2007, 2007.